

Supplementary Information

Parameterization of river incision models requires accounting for environmental heterogeneity: insights from the tropical Andes

**Benjamin Campforts^{1,2,3}, Veerle Vanacker⁴, Frédéric Herman⁵, Matthias Vanmaercke⁶, Wolfgang Schwanghart⁷,
Gustavo E. Tenorio^{8,9}, Patrick Willems¹⁰, and Gerard Govers⁹**

¹ Helmholtz Centre Potsdam, GFZ German Research Centre for Geosciences, Potsdam, Germany

² CSDMS, Institute for Arctic and Alpine Research, University of Colorado at Boulder, Boulder, CO, USA

³ Research Foundation Flanders (FWO), Egmontstraat 5, 1000 Brussels, Belgium

⁴ Earth and Life Institute, Georges Lemaître Centre for Earth and Climate Research, University of Louvain,
Place Louis Pasteur 3, 1348 Louvain-la-Neuve, Belgium

⁵ Institute of Earth Surface Dynamics, University of Lausanne, 1015 Lausanne, Switzerland

⁶ University of Liege, UR SPHERES, Department of Geography, Clos Mercator 3, 4000 Liège, Belgium

⁷ Institute of Environmental Science and Geography, University of Potsdam, Germany

⁸ Facultad de Ciencias Agropecuarias, Universidad de Cuenca, Campus Yanuncay, Cuenca, Ecuador

⁹ Department of Earth and Environmental Sciences, KU Leuven, Celestijnenlaan 200E, 3001 Leuven, Belgium

¹⁰ Department of Civil Engineering – Hydraulics Section, KU Leuven, Kasteelpark 40 box 2448, 3001 Leuven, Belgium

Correspondence to: Benjamin Campforts (benjamin.campforts@gfz-potsdam.de)

Contents of this file

Text S1

Figures S1 to S10

Tables S1 to S2

Additional supporting information (uploaded as separated .xlsx files)

Tables S3 to S4

Supplementary Information

Text S1: Topographic analysis

To compare inter-catchment variability of river steepness indices, the referenced concavity index (θ) is typically fixed to a value of 0.45 (DiBiase et al., 2010). In this section we explore whether assuming a fixed value for the concavity index is consistent with the diversity of river forms in the Paute basin. Our analysis relies on Bayesian optimization of the mn -ratio as implemented in the TopoToolbox function `mnoptim` (see also <https://topotoolbox.wordpress.com/2017/10/24/bayesian-optimization-of-the-mn-ratio/>).

The Paute river network is characterized by a major transient knickzone, situated close to the outlet of the basin (see main text for discussion). Including this knickzone in the mn -analysis would render the concavity to be significantly lower due to a major jump in the slope area profiles (Figure S3). It is known that there exists a positive trade-off between the concavity and the steepness of river profiles in transient regions (Vanacker et al., 2015). In order to facilitate the use of the stochastic stream power equation and ensure inter catchment comparability, we fixed the concavity to a value representative for the part of the river network being close to equilibrium. Therefore, we only considered the streams upstream of the two major knickzones in the Paute network, both likely originating from a major river reorganization in the recent geological past (<10 Ma Steinmann et al., 1999).

The Bayesian optimization procedure is based on the integral approach of longitudinal river profile analysis (chi-analysis) (Perron and Royden, 2013). Moreover, the optimization uses a cross-validation approach which randomly and repeatedly separates the drainage network into training and validation data. In one iteration, the mn -ratio is determined with the training data (~50% of the catchments) and is then evaluated with the remaining data (validation data) using the root mean squared error (RMSE). This approach is stochastic because at each iteration, different catchments are randomly selected. The RMSE for the same value of the concavity index may thus differ, which enables us to quantify the uncertainty of the optimal concavity. Bayesian optimization returns an optimal value of the $\theta = 0.42$ and is consistent with the value of 0.45 which is commonly used when modelling stochastic river incision (DiBiase and Whipple, 2011; Scherler et al., 2017). Uncertainty analysis (Figure S3) reveals that a range of mn -values between 0.35 and 0.5 is likely to result in equal model performance, further justifying adopting θ to 0.45 for the remainder of this study.

Chi-plots of drainage network for all individual sub catchments studied in this paper are shown in Figure S4.

Figure S5 illustrates the location of the digitized river sections to calibrate the river discharge-width relationship (main manuscript, Figure 4).

Figure S6 illustrates the procedure to downscale the coarse resolution (0.25°) WaterGAP3 reanalysis product for Ecuador using local rain gauge data and Figure S7 is an example of the daily discharge distribution for one catchment derived from WaterGAP data.

Figures S8 – S10 represent best model fits between CRN-derived erosion rates (E_{CRN}) and modelled river incision (E_{Mod}) using the scenarios listed in Table 4 of the main manuscript.

Supplementary Information

Table S1 Lithological erodibility index (L_A) based on the age of the lithological unit

| | L_A |
|----------------------|----------------------|
| Cambrium | 1 |
| Ordoviciium | 1.2 |
| Silurian | 1.3 |
| Devonian | 1.5 |
| Carboniferous | 1.8 |
| Permian | 2.5 |
| Permian/Triassic | 2.6 |
| Triassic | 2.7 |
| Triassic/Jurassic | 3 |
| Jurassic | 3.3 |
| Jurassic/Cretaceous | 3.7 |
| Cretaceous | 4.2 |
| Cretaceous/Paleogene | 4.6 |
| Paleogene | 5.2 |
| Paleogene/Neogene | 5.5 |
| Neogene | 5.8 |
| Neogene/Quaternary | 5.9 |
| Quaternary | 6 |

Table S2 Lithological erodibility index (L_L) per lithology, adjusted from on Aalto et al. (2006)

| Igneous | L_L | Metamorphic | L_L | Strong sedimentary | L_L | Unconsolidated | L_L |
|------------------------|----------------------|------------------------|----------------------|---------------------------|----------------------|-----------------------|----------------------|
| Adamellite | | Gneiss | | Limestone | | Alluvial deposits | |
| Diorite | | Amphibolite | | Massive greywacke | 4 | Colluvial deposits | |
| Dolerite | | Chert | 2 | Massive mudstone | | Estuarine deposits | 12 |
| Diabase | | Migmatite | | Massive sandstone | | Marine deposits | |
| Gabbro | | Serpentinite | | | | Laterite | |
| Granite | 2 | | | | | | |
| Granodiorite | | Metasedimentary | | Weak sedimentary | | | |
| Granophyre | | Quartzite | 2 | Conglomerates | | | |
| Ophiolite | | Meta lava | 3 | Pyroclastic | 10 | | |
| Pegmatite | | Schist | 4 | Shale | | | |
| Porphyry | | Slate | | Weathered sandstone | | | |
| Ultramafic | | | | Loose volcanic deposits | 12 | | |
| Andesite | | | | | | | |
| Basaltic Lava Rocks | 3 | | | | | | |
| Ignimbrite | | | | | | | |
| Nepheline | | | | | | | |

Supplementary Information

Table S3 Lithostratigraphic data

See file “TableS3.xlsx”

Table S4 Data PRECUPA

See file “TableS4.xlsx”

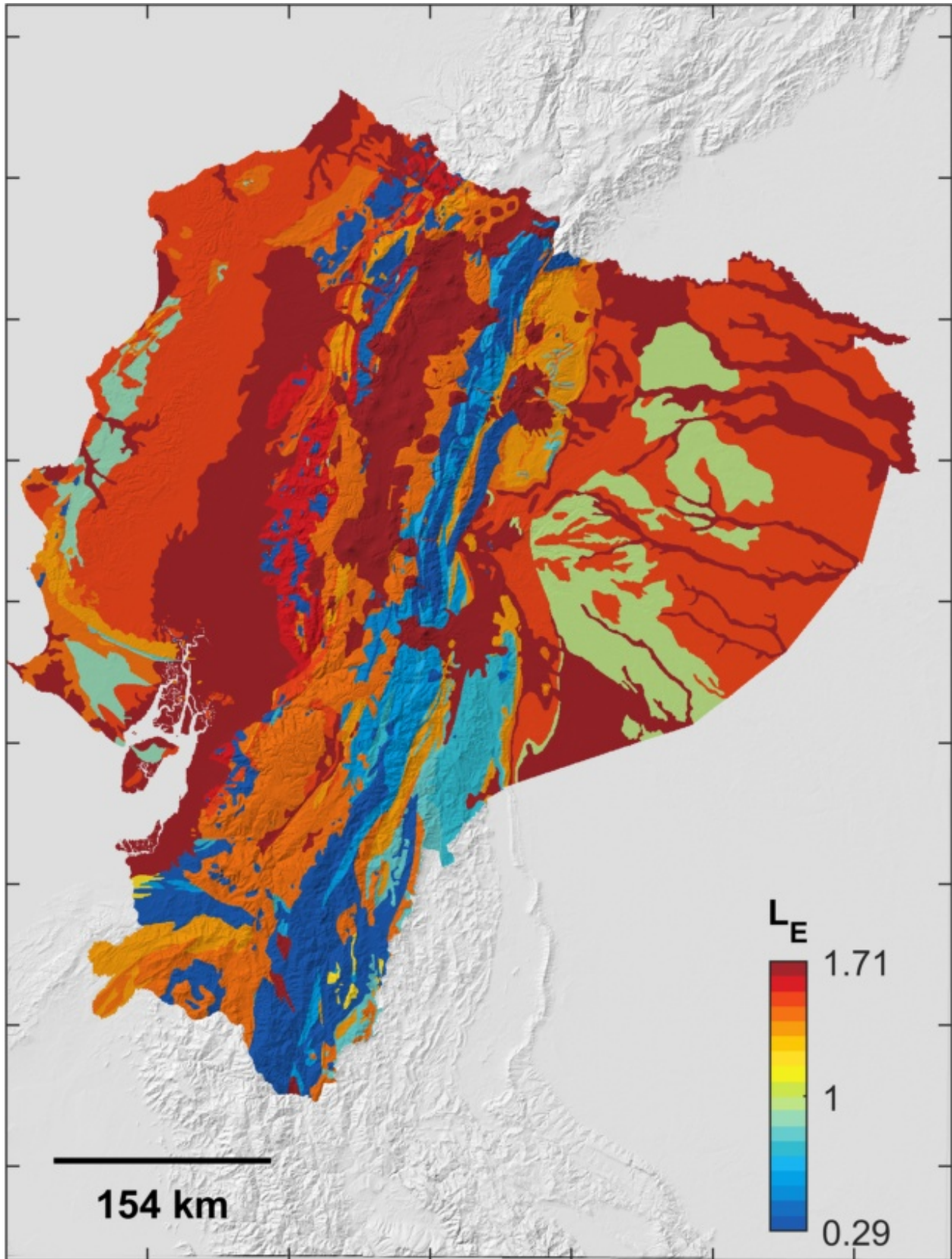


Figure S1 Erodibility map for Ecuador. Regionally constrained lithological erodibility index (L_E) derived from the 1M geological map of Ecuador (Egüez et al., 2017) and applying Eq. 15, overlain on hillshade map based on the 30 m SRTM v3 DEM (Farr et al., 2007). The map is produced with TopoToolbox (Schwanghart and Scherler, 2014).

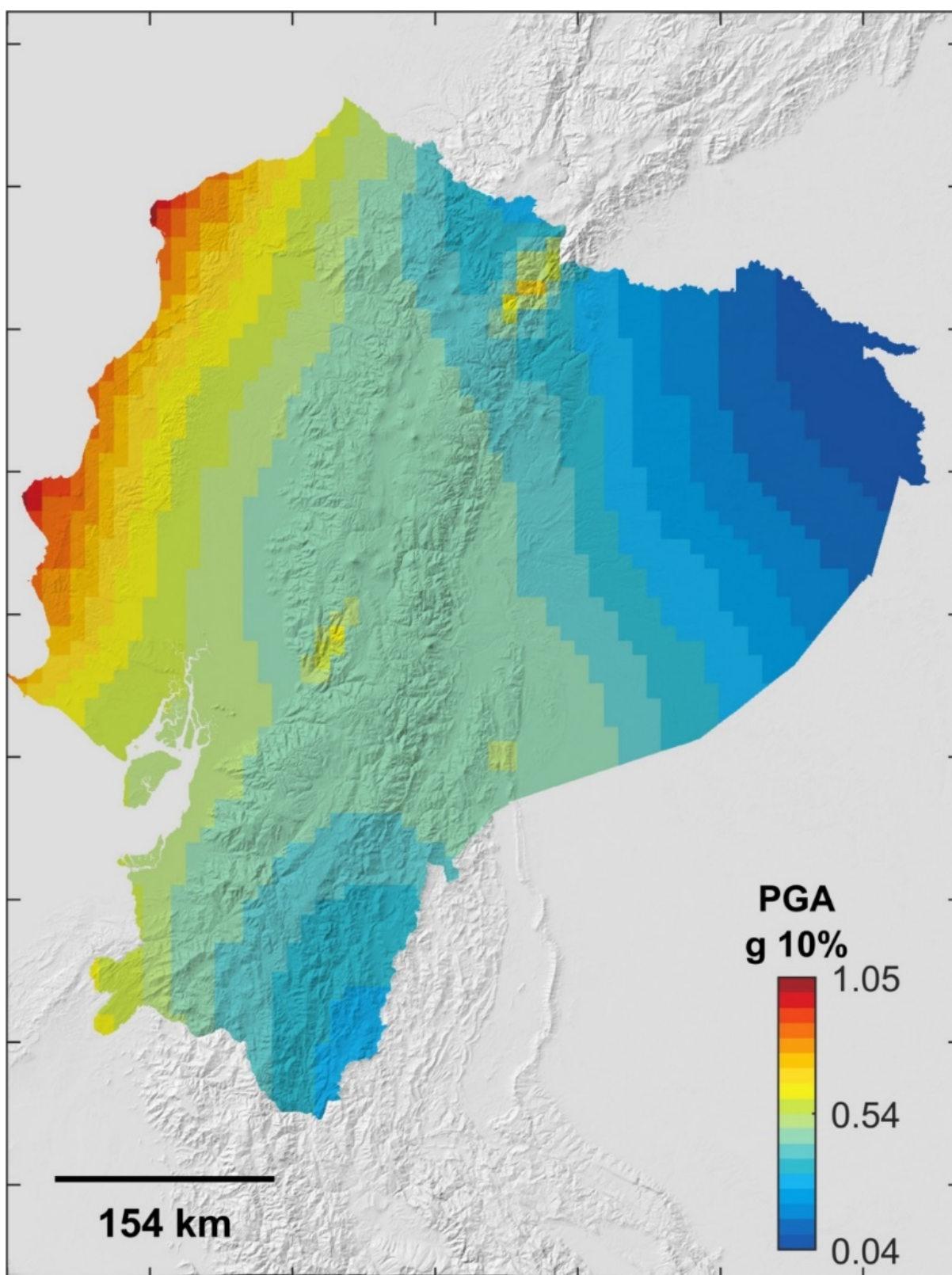


Figure S2 Peak Ground Acceleration (PGA) map for Ecuador. PGA (g) derived from Petersen et al. (2018) overlain on hillshade map based on the 30 m SRTM v3 DEM (Farr et al., 2007). PGA data available through ScienceBase (doi: 10.5066/F7WM1BK1). The map is produced with TopoToolbox (Schwanghart and Scherler, 2014).

Supplementary Information

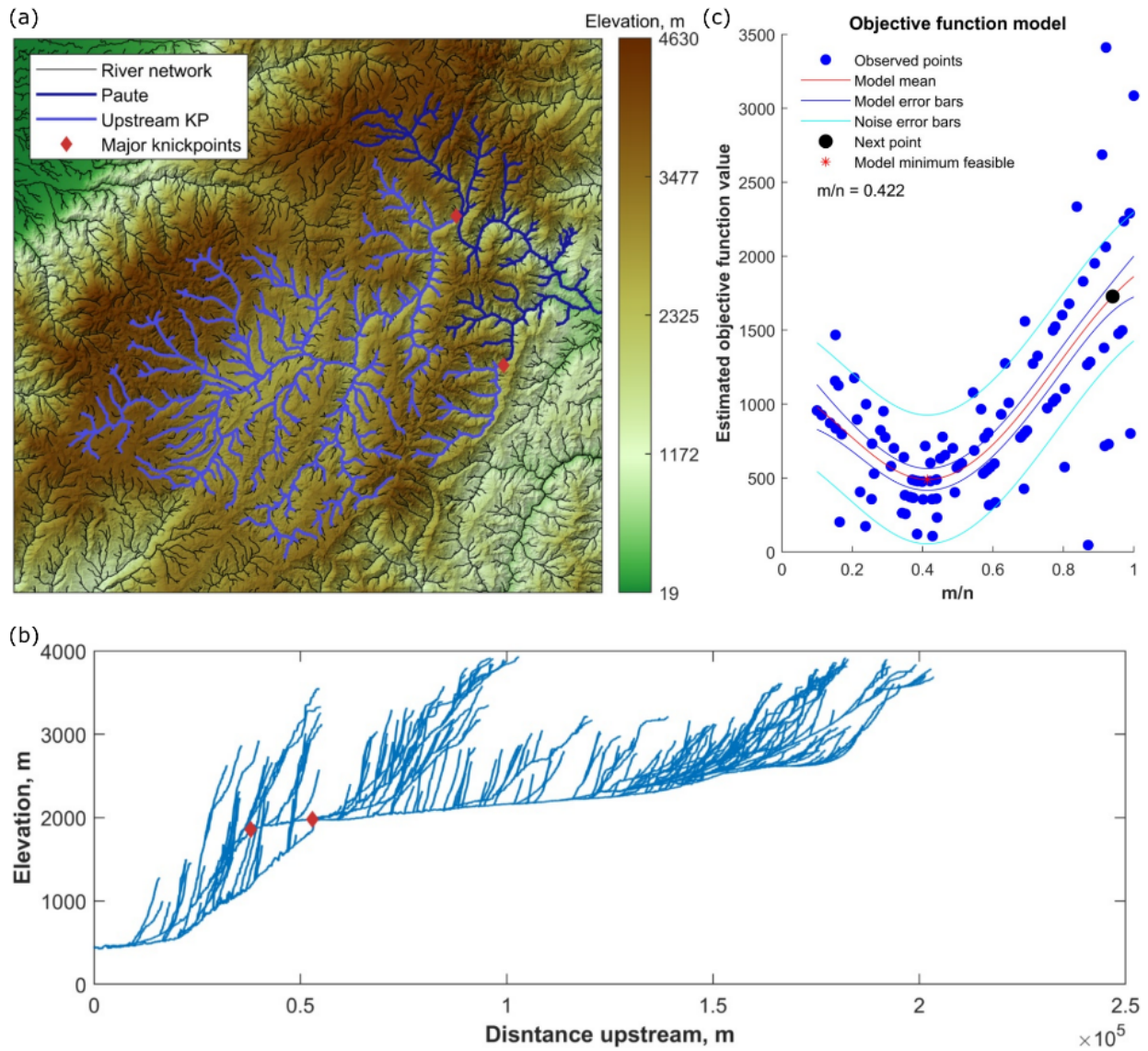


Figure S3: Constraining the concavity index of the Paute catchment using an objective function model. (a) River network with major knickpoints indicated as red diamonds, overlain on hillshade map based on the 30 m SRTM v3 DEM (Farr et al., 2007), (b) Longitudinal river profiles of the Paute drainage network. (c) Bayesian optimization of mn -ratio for the stream network upstream of the two major knickzones. Mapping and analysis are performed using TopoToolbox (Schwanghart and Scherler, 2014).

Supplementary Information

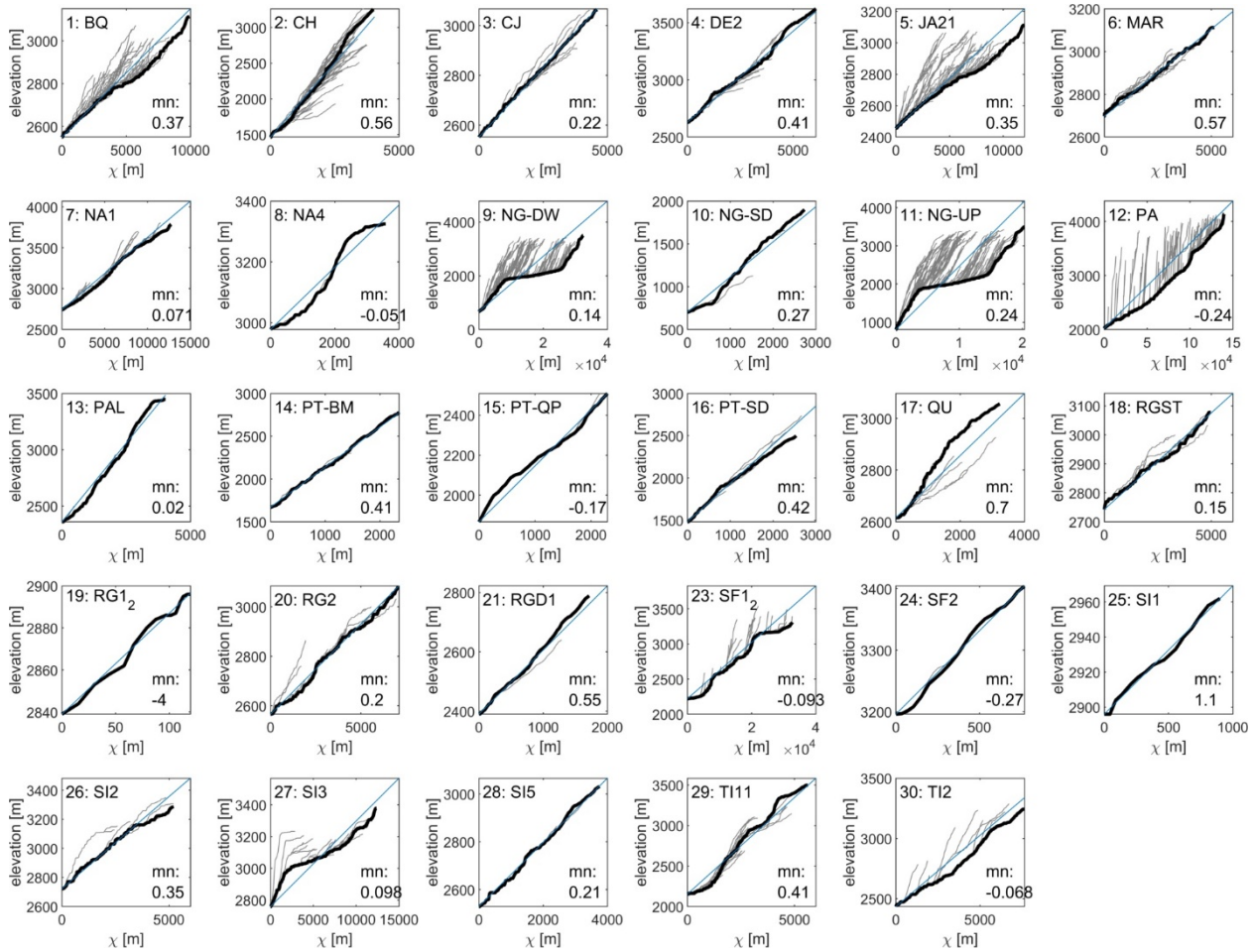


Figure S4: Chi-plots of drainage networks form studied sub-catchments. *mn*-value calculated using the chiplot function in TopoToolbox (Schwanghart and Scherler, 2014), assuming a critical drainage area of 0.5 km².

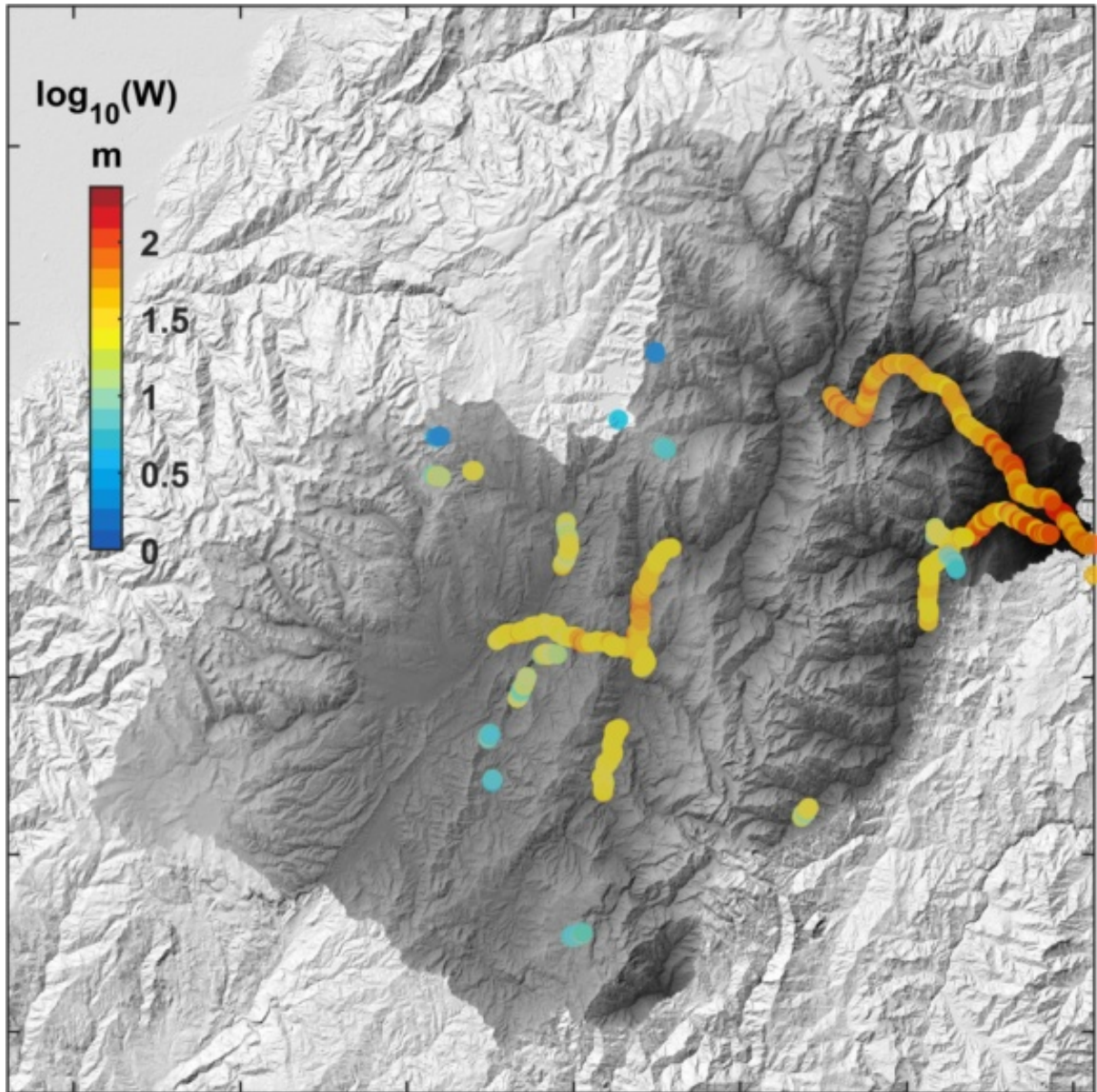


Figure S5: Sections of digitized bankfull river width. Mapped river width for ca. 120 km of channels overlain on hillshade map based on the 30 m SRTM v3 DEM (Farr et al., 2007). River width was digitized in Google Earth©, using the ChanGeom toolset (Fisher et al., 2013). The map is produced with TopoToolbox (Schwanghart and Scherler, 2014).

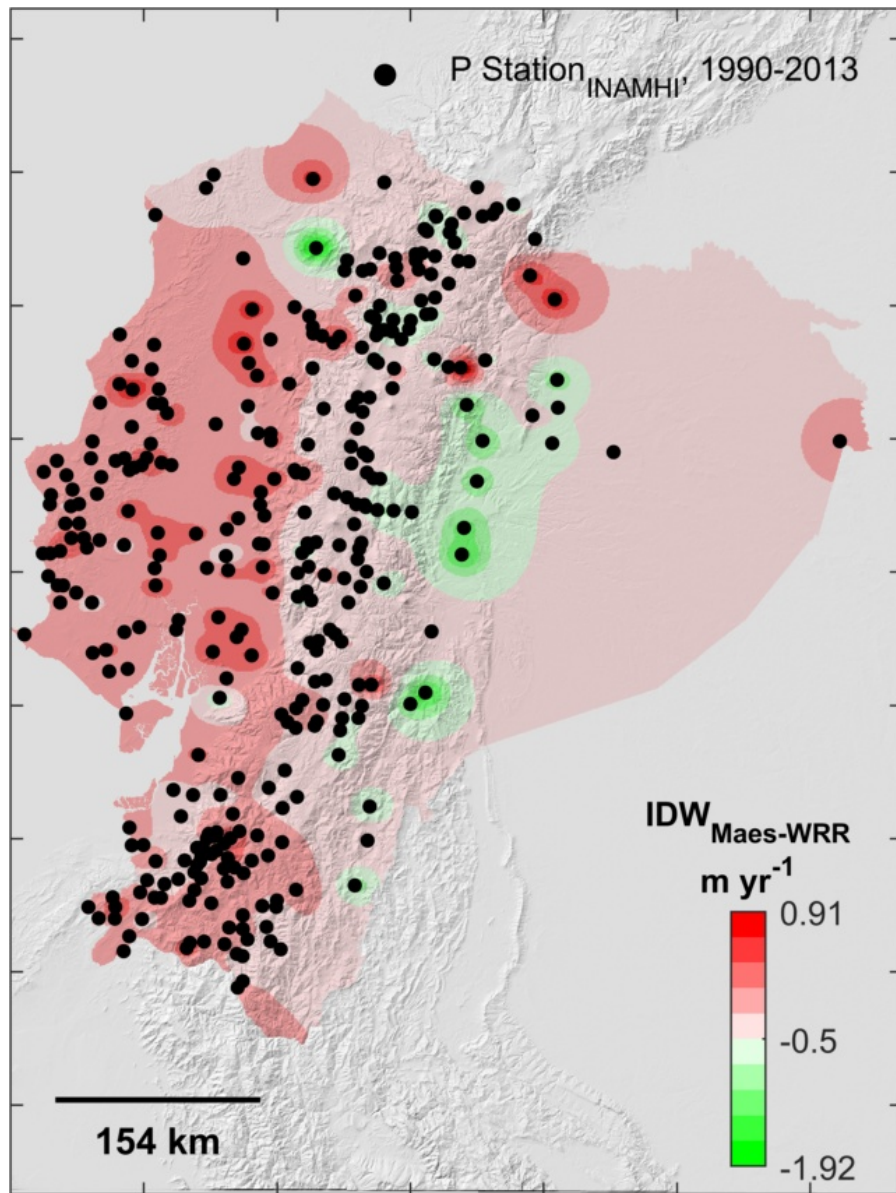


Figure S6: Downscaling of the coarse resolution (0.25°) WaterGAP3 reanalysis product for Ecuador using local rain gauge data. The colors represent an Inverse Distance Weighting (IDW) interpolation of the difference between rain gauge data (INAMHI, available from <http://www.serviciometeorologico.gob.ec/biblioteca/>) and WRR2-WaterGAP3 mean annual precipitation. The interpolation is overlain on a hillshade map based on the 30 m SRTM v3 DEM (Farr et al., 2007). WaterGAP3 data available from earth2observe.eu. The map is produced with TopoToolbox (Schwanghart and Scherler, 2014).

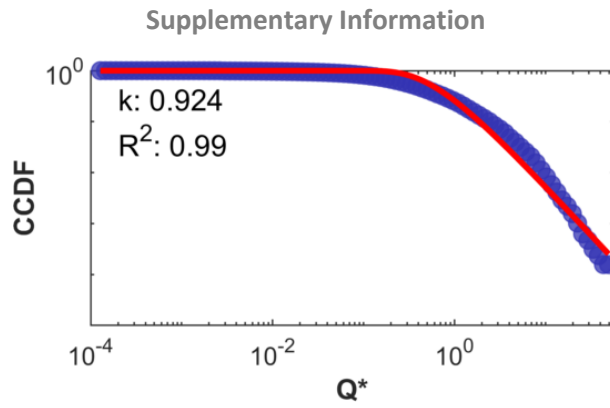


Figure S7: Example of daily discharge distribution derived from WaterGAP data. Daily discharge distribution (blue dots) derived at the outlet of one basin (NG-DW) using the downscaled WaterGAP data. The red curve depicts the fitted *ccdf* function (Eq. (14)) and its corresponding discharge variability coefficient (*k*). An overview of *k*-values for all sub-catchments is provided in Table 2.

Supplementary Information

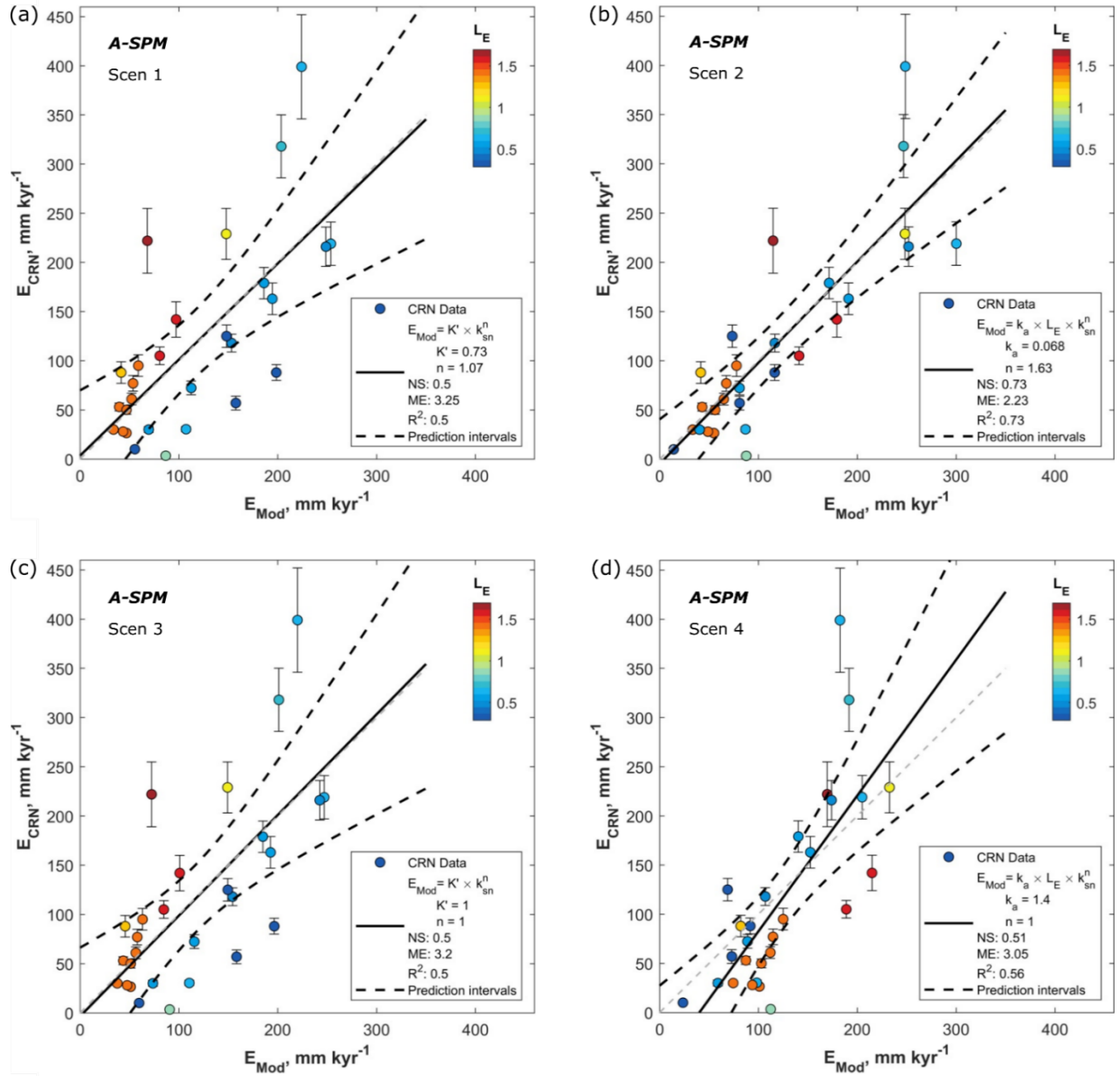


Figure S8: Best fit between CRN-derived erosion rates (E_{CRN}) and modelled river incision (E_{Mod}) using the area-based Stream Power Model (A-SPM). (a) A-SPM, scenario 1 assuming a uniform lithology. Observations are coloured according to the average lithological erodibility of the catchment ($\overline{L_E}$). Low values for $\overline{L_E}$ represent strong rocks, resistant to erosion. High values for $\overline{L_E}$ represent weak rocks, susceptible to erosion. Modelled erosion rates for catchments consisting of strong rocks (blue colors) are mostly over predicted and plot below the 1:1 line. Modelled erosion rates for catchments consisting of weak rocks (red colors) are mostly under predicted and plot above the 1:1 line. (b) A-SPM, scenario 2 where spatially variable lithological erodibility is explicitly accounted for in the A-SPM. (c) A-SPM, scenario 3 similar to scenario 1 but with the slope exponent, n fixed to 1. (d) A-SPM, scenario 4 similar to scenario 2 but with the slope exponent, n fixed to 1. Catchment specific values for $\overline{L_E}$ are listed in Table 2, while the model parameters are listed in Table 4.

Supplementary Information

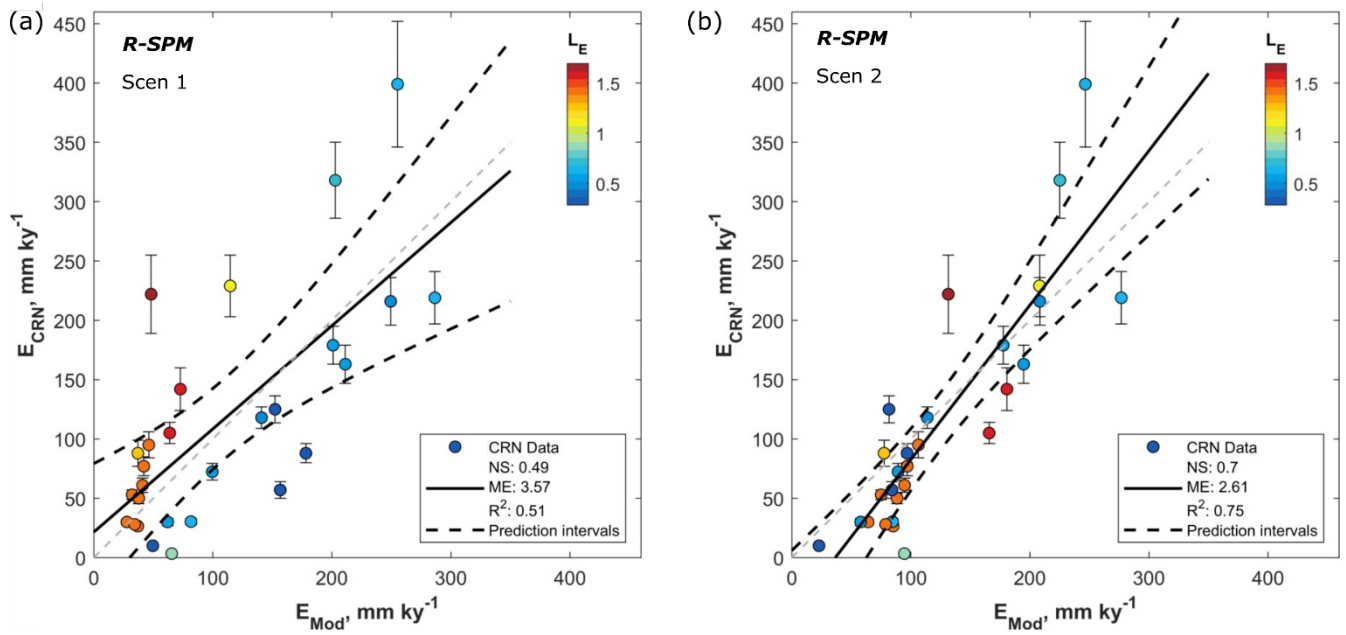


Figure S9: Best fit between CRN-derived erosion rates (E_{CRN}) and modelled river incision (E_{Mod}) using the runoff based Stream Power Models. (a) R-SPM, scenario 1 assuming average catchment runoff (\bar{R}) values and uniform lithological erodibility. (b) R-SPM, scenario 2 assuming average catchment lithological erodibility (\bar{L}_E) and runoff (\bar{R}) values. Catchment average values for \bar{L}_E and \bar{R} are listed in Table 2. An overview of all model parameter value and performance metrics is given in Table 4 of the main manuscript.

Supplementary Information

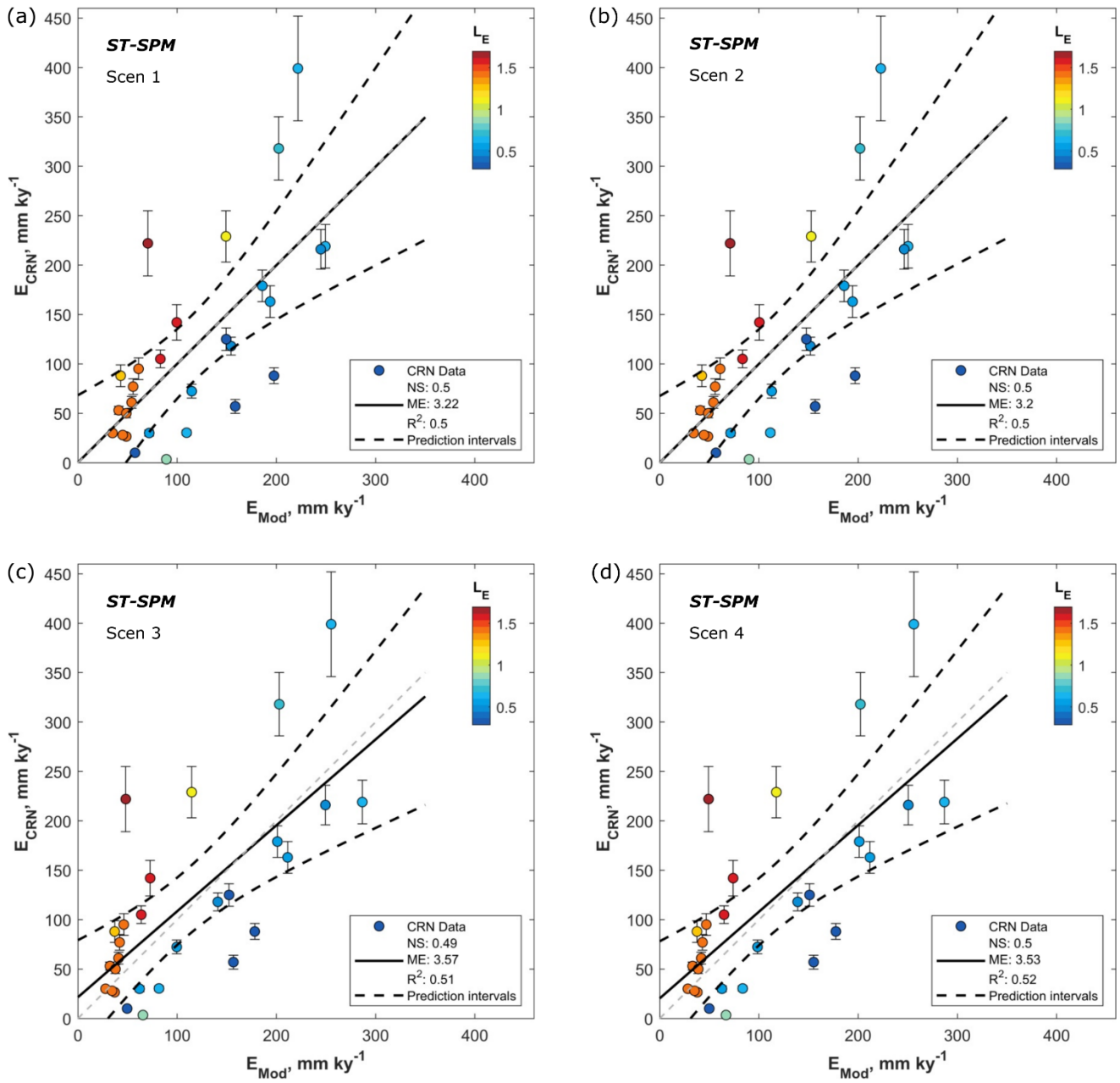


Figure S10: Best fit between CRN-derived erosion rates (E_{CRN}) and modelled river incision (E_{Mod}) using the Stochastic-Threshold Stream Power Models (a) ST-SPM, scenario 1 assuming a uniform lithological erodibility ($\overline{L_E}$), uniform runoff (\overline{R}) and a uniform discharge variability coefficient (k). (b) ST-SPM, scenario 2 assuming a uniform lithological erodibility ($\overline{L_E}$), uniform runoff (\overline{R}) and catchment specific values for the discharge variability coefficient (k). (c) ST-SPM, scenario 3 assuming a uniform lithological erodibility ($\overline{L_E}$), catchment specific values for runoff (\overline{R}) and a uniform discharge variability coefficient (k). (d) ST-SPM, scenario 4 assuming a uniform lithological erodibility ($\overline{L_E}$), catchment specific values for runoff (\overline{R}) and catchment specific values for the discharge variability coefficient (k).

Supplementary Information

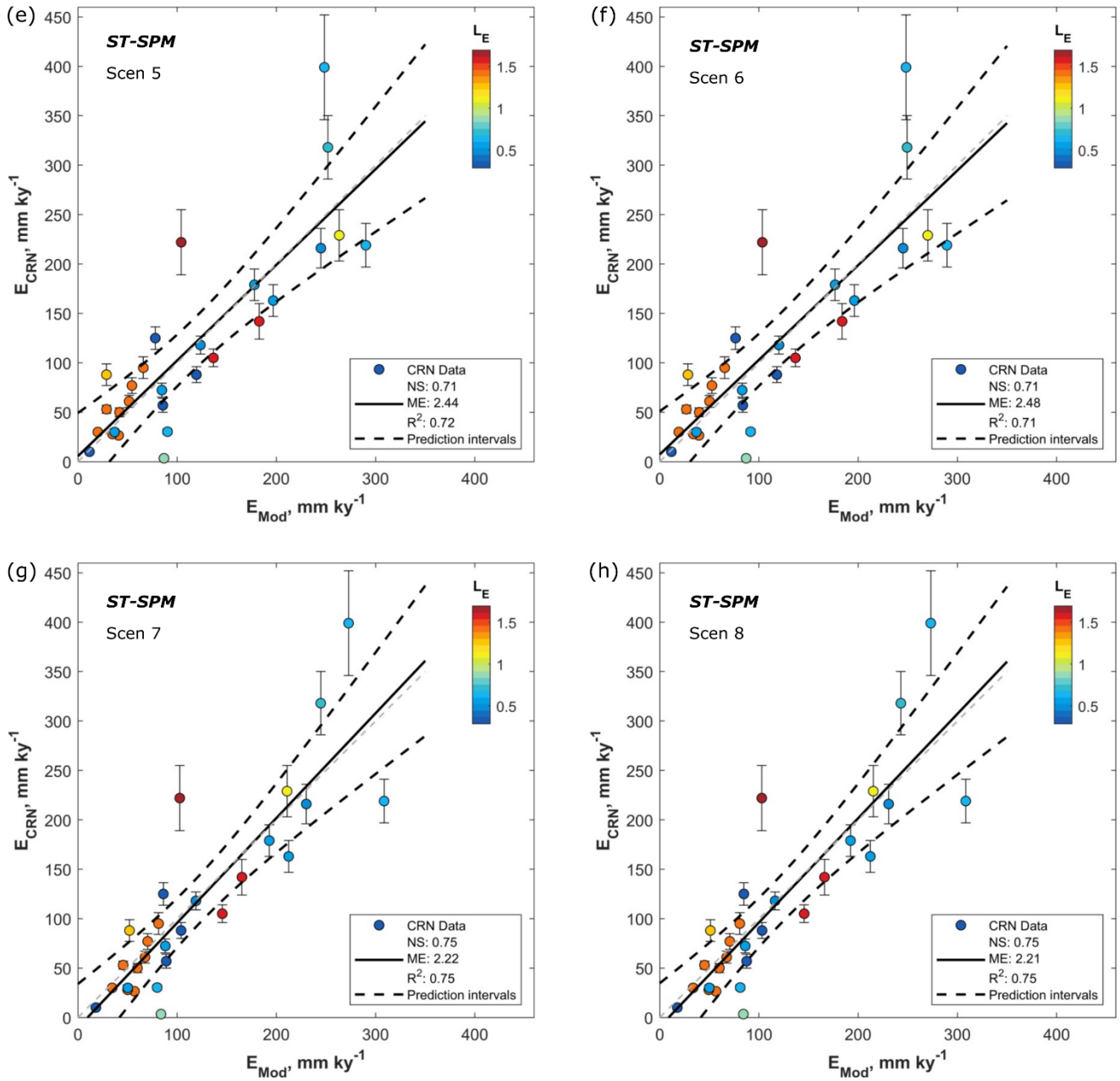


Figure S10 (continued)

(e) ST-SPM, scenario 5 assuming catchment specific values for erodibility ($\overline{L_E}$), uniform runoff (\overline{R}) and a uniform discharge variability coefficient (k). (f) ST-SPM, scenario 6 assuming catchment specific values for erodibility ($\overline{L_E}$), uniform runoff (\overline{R}) and catchment specific values for the discharge variability coefficient (k). (g) ST-SPM, scenario 7 assuming catchment specific values for erodibility ($\overline{L_E}$), catchment specific values for runoff (\overline{R}) and a uniform discharge variability coefficient (k). (h) ST-SPM, scenario 8 assuming catchment specific values for erodibility ($\overline{L_E}$), catchment specific values for runoff (\overline{R}) and catchment specific values for the discharge variability coefficient (k). Catchment average values for $\overline{L_E}$, \overline{R} and k are listed in Table 2. An overview of all model parameter value and performance metrics is given in Table 4 of the main manuscript.

Supplementary Information

References SI

- DiBiase, R.A., Whipple, K.X., 2011. The influence of erosion thresholds and runoff variability on the relationships among topography, climate, and erosion rate. *J. Geophys. Res.* 116, F04036. <https://doi.org/10.1029/2011JF002095>
- DiBiase, R.A., Whipple, K.X., Heimsath, A.M., Ouimet, W.B., 2010. Landscape form and millennial erosion rates in the San Gabriel Mountains, CA. *Earth Planet. Sci. Lett.* 289, 134–144. <https://doi.org/10.1016/j.epsl.2009.10.036>
- Egüez, A., Gaona, M., Albán, A., 2017. Mapa geológico de la República del Ecuador, Escala 1: 1.000. 000. Quito.
- Farr, T.G., Rosen, P.A., Caro, E., Crippen, R., Duren, R., Hensley, S., Kobrick, M., Paller, M., Rodriguez, E., Roth, L., Seal, D., Shaffer, S., Shimada, J., Umland, J., Werner, M., Oskin, M., Burbank, D., Alsdorf, D., 2007. The Shuttle Radar Topography Mission. *Rev. Geophys.* 45, RG2004. <https://doi.org/10.1029/2005RG000183>
- Fisher, G.B., Bookhagen, B., Amos, C.B., 2013. Channel planform geometry and slopes from freely available high-spatial resolution imagery and DEM fusion: Implications for channel width scalings, erosion proxies, and fluvial signatures in tectonically active landscapes. *Geomorphology* 194, 46–56. <https://doi.org/10.1016/j.geomorph.2013.04.011>
- Perron, J.T., Royden, L., 2013. An integral approach to bedrock river profile analysis. *Earth Surf. Process. Landforms* 38, 570–576. <https://doi.org/10.1002/esp.3302>
- Petersen, M.D., Harmsen, S.C., Jaiswal, K.S., Rukstales, K.S., Luco, N., Haller, K.M., Mueller, C.S., Shumway, A.M., 2018. Seismic Hazard, Risk, and Design for South America. *Bull. Seismol. Soc. Am.* 108, 781–800. <https://doi.org/10.1785/0120170002>
- Scherler, D., DiBiase, R.A., Fisher, G.B., Avouac, J.-P., 2017. Testing monsoonal controls on bedrock river incision in the Himalaya and Eastern Tibet with a stochastic-threshold stream power model. *J. Geophys. Res. Earth Surf.* 122, 1389–1429. <https://doi.org/10.1002/2016JF004011>
- Schwanghart, W., Scherler, D., 2014. Short Communication: TopoToolbox 2 - MATLAB-based software for topographic analysis and modeling in Earth surface sciences. *Earth Surf. Dyn.* 2, 1–7. <https://doi.org/10.5194/esurf-2-1-2014>
- Steinmann, M., Hungerbühler, D., Seward, D., Winkler, W., 1999. Neogene tectonic evolution and exhumation of the southern Ecuadorian Andes: a combined stratigraphy and fission-track approach. *Tectonophysics* 307, 255–276. [https://doi.org/10.1016/S0040-1951\(99\)00100-6](https://doi.org/10.1016/S0040-1951(99)00100-6)
- Vanacker, V., von Blanckenburg, F., Govers, G., Molina, A., Campforts, B., Kubik, P.W., 2015. Transient river response, captured by channel steepness and its concavity. *Geomorphology* 228, 234–243. <https://doi.org/10.1016/j.geomorph.2014.09.013>